Environmental Science
Processes & Impacts

Accepted Manuscript

This is an *Accepted Manuscript*, which has been through the Royal Society of Chemistry peer review process and has been accepted for publication.

Accepted Manuscripts are published online shortly after acceptance, before technical editing, formatting and proof reading. Using this free service, authors can make their results available to the community, in citable form, before we publish the edited article. We will replace this *Accepted Manuscript* with the edited and formatted *Advance Article* as soon as it is available.

You can find more information about *Accepted Manuscripts* in the Information for Authors.

Please note that technical editing may introduce minor changes to the text and/or graphics, which may alter content. The journal's standard Terms & Conditions and the Ethical guidelines still apply. In no event shall the Royal Society of Chemistry be held responsible for any errors or omissions in this *Accepted Manuscript* or any consequences arising from the use of any information it contains.

ROYAL SOCIETY OF CHEMISTRY

rsc.li/process-impacts

Graphical and textual abstract

Environmentally Persistent Free Radicals (EPFRs) have been found at a number of Superfund sites. Surrugate based Fe-loaded smectite clay showed a reduction in Fe (III) content after reaction with model organic contaminant (phenol) which led to the formation of EPFRs

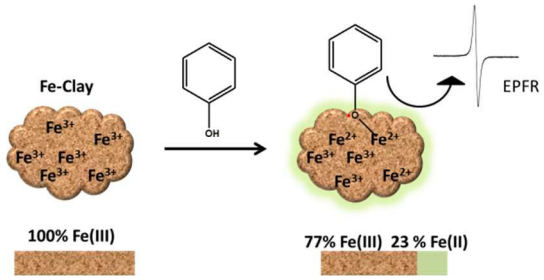

Environmental Science: Processes & Impacts Accepted Manuscript

Environmental Impact

This study presents a systematic approach to studying EPFRs by applying a range of analytical methods to a well-controlled environmental surrogate system of Fe-loaded montmorillonite clay. The goals of this work are to gain a molecular level understanding of the EPFR formation, the influence of environmental conditions on EPFR stability, and also to investigate the frequency with which EPFRs are formed per each reduction occurring on the redox center. The results of this study reveal that (i) EPFRs can be formed at environmentally relevant conditions without the need for a biotic pathway, (ii) EPFR formation is a rare event compared to the number of redox centers reduced, and (iii) environmental conditions play a major role in determining EPFR stability.

Environmental Science: Processes & Impacts Accepted Manuscript

Journal Name

ARTICLE

Formation of Environmentally Persistent Free Radical (EPFR) in Iron(III) Cation-Exchanged Smectite Clay

Ugwumsinachi G. Nwosu,[ab] Amitava Roy,[c] Albert Leo N. dela Cruz,[d] Barry Dellinger,[ab] and Robert Cook.[ab]*

Received 00th January 20xx,
Accepted 00th January 20xx

DOI: 10.1039/x0xx00000x

www.rsc.org/

Environmentally persistent free radicals (EPFRs) have been found at a number of Superfund sites, with EPFRs being formed via a proposed redox process at ambient environmental conditions. The possibility of such a redox process taking place at ambient environmental conditions is studied utilizing a surrogate soil system of phenol and iron(III)-exchanged calcium montmorillonite clay, Fe(III)CaM. Sorption of phenol by the Fe(III)CaM is demonstrated by Fourier-transformed infra-red (FT-IR) spectroscopy, as evidenced by the peaks between 1345 cm^{-1} and 1595 cm^{-1}, and at lower frequencies between 694 cm^{-1} and 806 cm^{-1}, as well as X-ray diffraction (XRD) spectroscopy, as shown by an increase in interlayer spacing within Fe(III)CaM. The formation and characterization of the EPFRs is determined by electron paramagnetic resonance (EPR) spectroscopy, showing phenoxyl-type radical with a g-factor of 2.0034 and $\Delta H_{P\text{-}P}$ of 6.1 G at an average concentration of 7.5×10^{17} spins/g. EPFRs lifetime data are indicative of oxygen and water molecules being responsible for EPFR decay. The change in the oxidation state of the iron redox center is studied by X-ray absorption near-edge structure (XANES) spectroscopy, showing that 23% of the Fe(III) is reduced to Fe(II). X-ray photoemission spectroscopy (XPS) results confirm the XANES results. These findings, when combined with the EPFR concentration data, demonstrate that the stoichiometry of the EPFR formation under the conditions of this study is 1.5×10^{-2} spins/Fe(II) atom.

1. Introduction

Clay minerals are important components of soils and act as a potential reservoir of metals and toxic organic pollutants.[1,2] Sorption of polycyclic aromatic hydrocarbons (PAHs) and chlorinated aromatic hydrocarbons to clay minerals has been used to remediate organic pollutants;[2,3] however, the possible formation

[a] Louisiana State University, Department of Chemistry, Baton Rouge, LA 70803, United States.
[b] Louisiana State University Superfund Research Center, Baton Rouge, Louisiana 70803, United States.
[c] Centre for Advanced Microstructures & Devices, Louisiana State University, 6980 Jefferson Highway, Baton Rouge, Louisiana 70806, United States.
[d] Department of Environmental Sciences, Louisiana State University, 1254 Energy Coast & Environment Bldg., Baton Rouge, LA 70803, United States.

† Footnotes relating to the title and/or authors should appear here.
Electronic Supplementary Information (ESI) available: [details of any supplementary information available should be included here]. See DOI: 10.1039/x0xx00000x

This journal is © The Royal Society of Chemistry 20xx

Environmental Science: Processes & Impacts Accepted Manuscript

of undesirable dioxins render this practice detrimental to the environment.[4,5] Organochlorinated contaminants, formed as products and by-products of such remediation processes, are not only toxic in their own right, but the intermediate reactions leading to their formation are also of major concern to environmental safety.[6,7] In particular, these intermediate processes result in the formation of surface-stabilized environmentally persistent free radicals (EPFRs).[2,8,9] Traditionally, EPFRs have been misidentified as molecular pollutants in soils and particulate matter.[10] The stability of an EPFR is associated with the ability of mostly aromatic organic contaminants to undergo chemisorption and form complexes with a redox (transition metal) centre, with the EPFR being formed through a single electron transfer.[9,11] In addition to EPFRs playing a role in the transformation of pollutants, radical processes involving EPFRs and organic compounds impact the formation of humic substances, and hence, carbon sequestration.[12] It has also been found that EPFR-containing particles can generate reactive oxygen species (ROS) which, in turn, may induce oxidative stress. This can occur in three steps: 1) EPFRs reduce molecular oxygen to superoxide, 2) the superoxide, through disproportion, forms hydrogen peroxide; 3) the reduced metal species formed via EPFR formation participate in Fenton chemistry which, in turn, generates ROS.[7] EPFRs have recently been found at elevated concentrations in numerous soil/sediment samples from a range of pentachlorophenol-polluted Superfund sites.[13,14] A detailed top-down study found that the EPFRs were almost solely associated with the clay/humic soil fraction.[14]

Other studies have shown that: 1) dioxin radicals can form in the presence of Cu(II) smectite montmorillonite clay mineral, [15] 2) pentachlorophenol (PCP) radical cations are generated in Fe(III)-montmorillonite clay,[2] and 3) transition metal centres in clay minerals play a key role in the formation of the intermediate radicals in the formation of dioxins.[2,5] However, these studies were carried out at conditions not relevant to the EPFR-contaminated Superfund sites as organic solvents were used and/or high temperature and reflux conditions were applied. Our previous investigations also demonstrated the catalytic role of transition metal centres, Cu(II) and Fe(III) supported on silica particles metal surfaces, in the formation of intermediate EPFRs.[9,11,16] While important, these studies did not address the type of conditions present at the Superfund sites in which soil EFPRs have been found.

With the remediation of EPFR-contaminated soil systems being the ultimate goal of this research, it is important to first gain a fundamental molecular level understanding of how EPFRs are formed in soils at environmental conditions. The soil matrix, however, due to its complexity, poses major technical challenges for modern molecular level analytical methods, thus a bottom-up approach is appropriate, in which a soil is broken down into its biological, organic, and inorganic components and the role of each of these components is determined individually and in combination with each other. In this effort to systematically reconstruct the geosorbant (here soil) and understand at a molecular level the mechanism of EPFR formation in contaminated soil systems, we report on the use of Fe(III) exchanged montmorillonite clay, designed to model the clay component of a real soil in which EPFR have been shown to concentrate.[14] Iron was chosen as the redox centre of interest as it was found to be the most abundant transition metal in the contaminated Superfund sites.[13] Phenol was utilized as a simplified model of organic contaminants as it is a well known soil contaminant itself and can be easily produced by microbial reductive dechlorination of chlorophenol and polychlorophenols in contaminated soils,[17] and is considered as priority pollutant by U.S. EPA.[18] The following analytical techniques were combined in this study: 1) Fourier transformed infrared (FTIR) spectroscopy and X-ray diffraction (XRD) to demonstrate the sorption of the model pollutant, phenol, 2) X-ray photoelectron spectroscopy (XPS) to study the changes in chemical environment of Fe species, the redox centre of interest in this study, and other elements in the clay, 3) electron paramagnetic resonance (EPR) spectroscopy for radical detection and quantification, and 4) X-ray absorption near edge structure (XANES) spectroscopy to investigate the redox change of the Fe centres. This non-biological approach offers insights into the mechanism of the EPFR formation in soils and allows one to measure EPFR lifetimes under environmentally relevant conditions.

2. Experimental

2.1 Materials

Smectite clay (CaM), STx-1b (Montmorillonite) with a cation exchange capacity (CEC) of 84.4 meq/100 g and a surface area of 83.79 ±0.22 m^2/g, was purchased from the Source Clay Repository (Purdue University, West Lafayette, IN). Iron(III) chloride, $FeCl_3$, was obtained from Sigma Aldrich, analytical grade phenol (loose crystal) was obtained from Mallinckrodt, and trace metal grade nitric acid, HNO_3, was obtained from Fisher Scientific.

Preparation of Fe-Exchanged Clay Samples: Cation-exchange was performed following well established protocols.[2,19] Briefly, a 4 g sample of clay was placed in a 250 mL beaker and mixed with 25 mL of 0.012 M $FeCl_3$ solution for proper hydration and dispersion. The resulting suspension was then diluted up to 100 mL with additional $FeCl_3$ solution and stirred for 48 h. The Fe(III) clay suspension was transferred to a dialysis tube and immersed into 18 MΩ•cm water. The water was replaced every 12 h in order to wash out free chloride ions associated with $FeCl_3$ until a negative $AgNO_3$ test. The resulting clay material (Fe(III)CaM) was filtered using a suction vacuum filtration set-up and allowed to dry for 48 h at 60 °C. The sample was then crushed and homogenized using mortar and pestle and utilized for subsequent experiments.

2.2 ICP-OES-Analysis

The metal content of the clay samples was determined by inductively coupled plasma optical emission spectroscopy (ICP-OES) using a Varian Vista-MPX CCD Simultaneous ICP-OES. For this analysis, a 0.2 g sample of clay was digested in 5 mL of concentrated HNO_3 for approximately 8 h, cooled, and the resultant digestate was diluted to a total volume of 50 mL with 18 MΩ•cm water and analyzed.

This journal is © The Royal Society of Chemistry 20xx

Environmental Science: Processes & Impacts Accepted Manuscript

2.3 Gas Phase Phenol Dosing of Clay Samples

Clay samples were dosed with phenol following a previously reported method.[14] Briefly, 50 mg of samples, contained in a 4 mm glass detachable bulb-shaped pyrex reactor with a protruding Suprasil® quartz EPR tube, were exposed to phenol at room temperature in vapor phase by dosing in a custom-made vacuum exposure system. Sample dosing commenced after the attainment of a ~10^{-2} mm Hg vacuum to allow the removal of interfering organic contaminants. Unreacted physisorbed phenol was evacuated by applying a vacuum of 10^{-2} mmHg. This procedure resulted in the production of four different samples, namely: pristine montmorillonite (PureCaM), phenol-exposed pristine montmorillonite (DosedCaM), Fe(III)-cation-exchanged montmorillonite (Fe(III)CaM), and phenol-exposed Fe(III)-cation-exchanged montmorillonite (DosedFe(III)CaM). All phenol-exposed samples were protected from light throughout the study.

2.4 Sample Exposures

Three different sample exposures were used in this study. First, the sample was simply left under vacuum. Secondly, the sample was exposed to ambient air. The third experiment involved exposing the sample to humid air inside a Model 3940 Series Forma Environmental Chamber with the relative humidity and temperature set at 75% and 25 °C, respectively.

2.5 Electron Paramagnetic Resonance (EPR) Spectroscopic Analysis

EPR measurements were conducted using a dual cavity Bruker EMX 10/2.7 EPR spectrometer with a X-band microwave frequency of 9.78 GHz at room temperature and spectra were recorded under the following instrumental conditions: sweep width of 150 G and 6000 G, attenuator of 20 dB, power of 2.03 mW, modulation frequency of 100 kHz, modulation amplitude of 4 G, sweep time of 41.94 s, time constant of 1.28 ms, conversion time of 20.48 ms, static field of 3460.059 G, centre field of 3488.00 G, receiver gain of 1.0 x 10^4, and a total of 5 scans. The instrument was calibrated with a 2,2-diphenyl-1-picrylhydrazyl (DPPH) standard.[11,20]

2.6 FTIR Analysis

Infrared spectra were collected on a Bruker Alpha or Tensor 27 Fourier transform infrared (FT-IR) spectrometer. Powdered clay samples were dispersed directly onto a Pike Miracle ATR cell sample plate as to cover the Pt-diamond crystal. Spectra acquisition was recorded within the frequency ranges of 400 cm^{-1} to 4000 cm^{-1} at a minimum resolution of 4 cm^{-1} by averaging 16 scans.

2.7 X-Ray Analysis

X-ray absorption near edge structure (XANES) spectra were obtained at the wavelength shifter Double Crystal Monochromator (WDCM) beam line of the J. Bennett Johnston, Sr., Center for Advanced Microstructures and Devices (CAMD) located on the 7 T wavelength shifter. Germanium 220 crystals were used in a Lemonnier-type monochomator with design modifications made at Bonn University, Germany. Iron metal foil was used for monochromator calibration at 7112 eV. Samples were prepared by spreading a few µm thick clay powders onto a Kapton™ tape. The measurements in fluorescence mode were made with a 13-element germanium solid state detector (Canberra Industries, Meridian, Connecticut, USA). Multiple scans (2-5 scans each) were performed at room temperature and were averaged using the Demeter software (Ravel and Newville, 2005). Spectra of reagent grade standards of Fe_2O_3, FeO and Fe_3O_4 were also collected for least squares fitting. The X-ray diffraction (XRD) data were collected on a PANalytical Empyrean diffractometer using the Cu Kα radiation of λ = 1.5419 Å within 2Θ scan range of 5 – 90°. The X-ray photoelectron spectroscopy (XPS) measurements were performed using the Kratos AXIS 165 XPS/AES system equipped with a monochromatic Al-Kα source and a charge neutralizer, at pass energy of 80 eV for high resolution scans. The step size of 0.05 eV was applied and shifts in binding energies were corrected with a 284.6 carbon 1s peak as internal reference.

3. Results and discussion

Our previous research on particulate matter ($PM_{2.5}$) proposed that EPFR formation involves an initial physisorption of an organic pollutant, followed by chemisorption and a concurrent single electron transfer process to an active redox (transition metal) centre.[9,11,16] In this study we wish to (i) determine if the same processes could take place on a very simple soil surrogate system, namely Fe(III)CaM, under ambient environmental conditions, (ii) monitor the sorption of the organic pollutant (in this case phenol), the formation of the EPFRs, and the reduction of the transition metal centre, (iii) quantify the amount of EFPRs formed and metal centres reduced, as well as (iv) determine the influence of environmental conditions on EPFR stability.

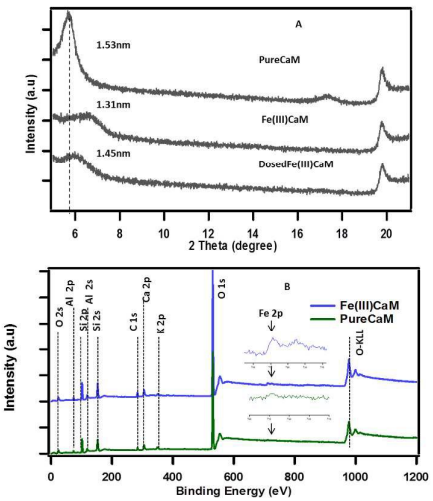

Fig. 1 XRD pattern spectra of A) PureCaM, Fe(III)CaM and DosedFe(III)CaM, B) XPS survey spectra of (Fe(III)CaM) and PureCaM. Experiment performed with 1.8 x 10^4 mg/kg Fe loading.

Environmental Science: Processes & Impacts Accepted Manuscript

Please do not adjust margins

3.1 PureCaM and Fe(III)CaM Characterization

As shown in Fig. 1A, a reduced basal spacing in the XRD pattern from 1.53 nm for the PureCaM sample to 1.31 nm for the Fe(III)CaM sample indicates the replacement of interlayer Ca(II) cations by Fe(III).[21] An XPS survey spectra (Fig. 1B) show intense oxygen peaks associated to the major silicate Si (2*s*, 2*p*) and aluminate Al (2*s*, 2*p*) metal framework that forms the tetrahedral and octahedral layers in calcium montmorillonite clay.[22] The Fe 2*p* region in the survey after cation exchange appears to intensify after treatment with Fe(III) (inset spectra). This is an indication of Fe(III) exchange with the Al(III) interstitial lattice sites of the octahedral aluminate clay layers.[23] Similarly, the intercalation and the replacement of calcium and other interlayer cations with by Fe(III) species are also known to be responsible for such changes.[24] Overall, these data strongly suggest that the Fe(III) introduced in the cation exchange procedure is interstitial in nature; however, the possibility of FeOOH coating a small percentage of the clay surface cannot be completely disregarded.

3.2 Phenol Sorption

The sorption of phenol to the clay samples following the dosing procedure was confirmed using FTIR spectroscopy by the presence of phenol vibrational frequencies in the phenol-dosed samples.

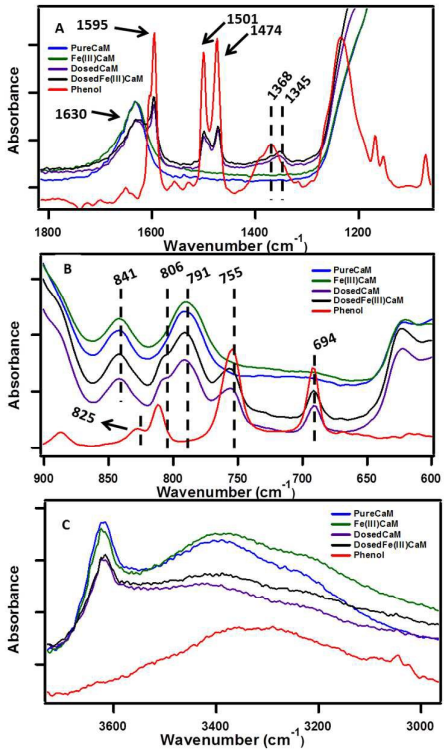

Fig. 2 FTIR spectra showing sorption of phenol at different wavenumbers, ranging from 4000 cm^{-1} to 600 cm^{-1}, with Fe loading of 1.8 x 10^4 mg/kg . (Expanded view)

The spectral regions presented in Fig. 2A and 2B are highly diagnostic of phenol sorption. In Fig. 2A sorption of phenol to the DosedCaM and DosedFe(III)CaM samples is shown via the absorption bands at 1595 cm^{-1}, 1501 cm^{-1}, 1474 cm^{-1}, and 1345 cm^{-1}. The double peaks at 1501 cm^{-1} and 1474 cm^{-1}, along with the peak at 1595 cm^{-1}, are all attributable to the carbon-carbon stretching vibration of phenol, while the bands at 1368 cm^{-1} and 1345 cm^{-1} for pure phenol, DosedCaM, and DosedFe(III)CaM are assignable to the in-plane -OH bending.[25-26] Other bands seen in Fig. 2B that are associated with the adsorption of phenol appear in the lower frequency region at 755 cm^{-1} and 694 cm^{-1} and correspond to the out-of-plane C–H bending.[26] Similarly, a shoulder peak at 806 cm^{-1}, typical of the aromatic C–H bending region, indicates adsorption of phenol to the metal cation.[26-27] The sorption of phenol is further supported by the increase in the basal spacing observed from the XRD patterns (*cf.* Fig. 1) between the Fe(III)CaM and DosedFe(III)CaM samples from 1.31 nm to 1.45 nm, respectively. Spectra shown in Fig. 2C reveal a broad and rather featureless envelope of peaks between 3200 cm^{-1} and 3583 cm^{-1} for all clay samples and pure phenol, which can be assigned to a number of different hydroxyl group types. The sharp peak at 3628 cm^{-1} for the clay samples can be assigned to the -OH groups associated with Si(IV) and Al(III) or Fe(III) in the tetrahedral and octahedral sheets.[28-30] Fig. 2C further shows the corresponding -OH bending absorption bands between 841 cm^{-1} and 791 cm^{-1} for octahedral cations (Si(IV), Al(III), and Fe(III)), mainly Al-OH-Fe and Al-OH-Mg.[24,28] In addition, H–O–H stretching vibrations from inherent and adsorbed interfacial water molecules and weak hydrogen bonding within the Si–O surfaces have also been known to show strong absorption bands within these regions.[28-31]

3.3 EPFR Formation and Analysis

The presence of organic radicals, EPFRs, were detected by EPR shortly after the dosing of the Fe(III)CaM with phenol.

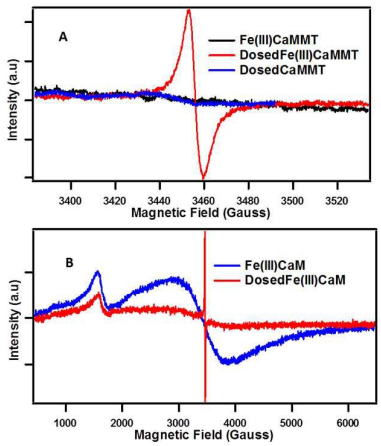

Fig. 3 EPFR generation: EPR spectra for Fe(III)CaM with Fe loading of 1.8 x 10^4 mg/kg and DosedFe(III)CaM at A) 150 G and B) 6000 G spectral width.

EPR Analysis: The EPR spectrum presented in Fig. 3A provides clear evidence of EPFR formation when Fe(III)CaM is dosed with phenol.

This journal is © The Royal Society of Chemistry 20xx

Environmental Science: Processes & Impacts Accepted Manuscript

Please do not adjust margins

The EPFR signal in Fig. 3A is a nearly symmetrical peak with the magnetic field centred at 3460 G, an average g-factor of 2.0034, and peak-to-peak line width (ΔHp-p) of ~6.1; these values correspond to an oxygen-centred phenoxyl-type organic radical.[11,16] The EPR spectrum at 6000 G, presented in Fig. 3B, provides further insight into the chemical environment of the unpaired electron. A broad peak at g-factor = 2.03 and a somewhat narrower peak towards the lower magnetic field at g-factor = 4.21 are attributed to low and high spin octahedral and tetrahedral paramagnetic Fe(III) ion sites, respectively.[32-33] The peak at g-factor = 2.03 is superimposed by the peak associated with the organic radical formation after phenol exposure.

The example of Fe(III) illustrates the importance of transition metal centres and their exact speciation. It is further supported by the fact that the DosedCaM system does not form EPFRs. While PureCaM does inherently possess Fe(III) centres, they are located at the enclosed inner lattice sites in the octahedral clay layer. This hinders phenol-Fe(III) interactions, preventing EPFR formation, as indicated by no radicals being detected in the DosedCaM system. This demonstrates that intercalated Fe(III) species are mainly responsible for the formation of the organic radicals through a single-electron oxidation of phenol.[11,16] Furthermore, a change in colour from brownish yellow for Fe(III)CaM to greyish green for the DosedFe(III)CaM also confirms the occurrence of a redox process; this has been previously observed for the Fe(III) reduction to Fe(II) in montmorillonite clays.[34]

3.4 Role of Redox Centres in EPFR Formation

The role of the Fe(III) redox centre was further studied by a combination of high resolution XPS and XANES.

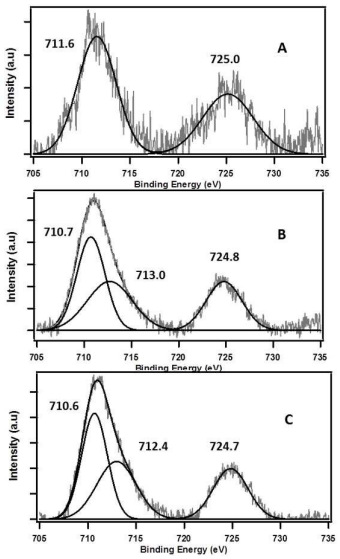

Fig. 4 Deconvoluted high resolution XPS spectra of Fe 2*p* binding energy peak regions for A) PureCaM, B) Fe(III)CaM, and C) DosedFe(III)CaM. Experiment performed with 1.8 x 10^4 mg/kg Fe loading.

High Resolution XPS: The high resolution XPS scans of the Fe 2*p* region in the survey scan in Fig. 1B can be employed to further explain the changes in the chemical state of Fe(III) after cation exchange and subsequent radical formation. Fig. 4A-C highlights the Fe $2p_{3/2}$ and Fe $2p_{1/2}$ binding energy peaks of iron. The peaks at 711.6 and 725.0 eV for the PureCaM are assignable to the structural Fe, confirming that Fe(II) and Fe(III) are embedded in the montmorillonite lattice.[35] After cation exchange with Fe(III), the Fe $2p_{1/2}$ peak remains nearly unchanged (724.8 eV for Fe(III)CaM and 724.7 eV for DosedFe(III)CaM). On the other hand, the Fe $2p_{3/2}$, which is considered to be the main Fe 2*p* peak, partitions into two sub-peaks positioned at 710.7 eV and 713.0 eV, that may be attributed to structural and intercalated Fe species, respectively.[35] Upon dosing with phenol, the position of the peak ascribed to the intercalated Fe(III) shows a 0.6 eV shift from 713.0 eV to 712.4 eV. This suggests a change in chemical state of Fe(III), consistent with a reduction of Fe(III) to Fe(II)

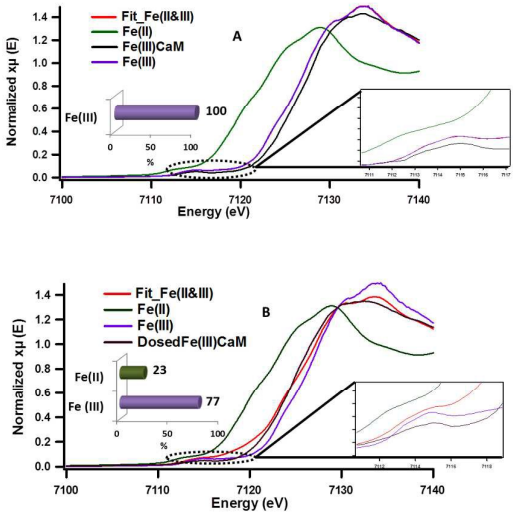

Fig. 5 XANES spectra showing the changes in redox state of iron pre- and post-phenol dosing A) Iron standards (Fe(II) and Fe(III)), Fe(III)CaM, and the Fe(III)CaM Fit, B) Iron standards (Fe(II) and Fe(III)), Fe(III)CaM dosed with phenol, and the Fe(III)CaM dosed with phenol Fit. Experiment performed with 1.8 x 10^4 mg/kg Fe loading.

XANES Studies: In order to further confirm the mechanism by which EPFRs are formed, Fe(III)CaM and DosedFe(III)CaM samples were analyzed by XANES, with the focus on the Fe redox centre. The data in Fig. 5 show, based on the K-edge energy shift, the partial reduction of Fe(III) to Fe(II) (100% Fe(III) for Fe(III)CaM and 77%Fe(III) and 23%Fe(II) for DosedFe(III)CaM) after phenol dosing. These data, when synthesized with the FT-IR and EPR data discussed above, lead to the mechanism proposed in Scheme 1, whereby the initial phenol adsorption in the Fe(III)-exchanged clay results in the abstraction of a hydrogen atom from phenol and a single electron transfer from the phenol molecule to the Fe(III) centre, leading to the EPFR formation. This mechanism is consistent with the EPFR formation mechanism proposed for $PM_{2.5}$.[36-37] The XANES data presented in Fig. 5 reveal additional mechanistic information beyond the oxidation state of Fe redox centres in the

Environmental Science: Processes & Impacts Accepted Manuscript

Please do not adjust margins

formation of EPFRs. Least squares fitting of the spectra demonstrates a decrease in the main-edge intensity of the spectra for the probed post phenol-dosed sample (Fit_Fe(II&III)) compared to the iron standards (Fe(II) and Fe (III)). This suggests an alteration typical of the octahedral or near octahedral coordination environment of Fe in the post phenol-dosed sample.[38-42] A significant edge shift from 7125.5 eV to 7124.0 eV and 7122 eV to 7120 eV at the centre and the base of the K-edge towards the Fe(II) energy for the phenol-dosed sample (Fit_Fe(II&III)), when compared to the Fe(III) standard, provides further strong evidence of the change in oxidation state of iron from Fe(III) to Fe(II).[38-41]

Scheme 1. General mechanism for EPFR formation with phenol on Fe(III)CaM

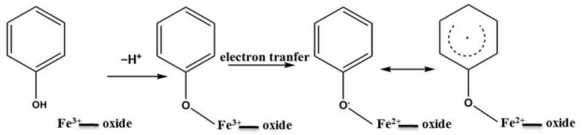

The expanded insets of the Fig. 5A-B show the emergence of an intense and broad peak in the post phenol-dosed sample spectrum DosedFe(III)CaM and in its spectral fit (Fit_Fe(II&III)). It results in a slight deviation from the pre-edge centroid position. This type of shift has been previously associated with a change in oxidation state of Fe(III).[38-42] However, further explanation can be ascribed to the distortion in the coordinating ligands after chemisorption, with the subsequent replacement of ligating species, such as -OH and H_2O, following a single electron transfer from phenol molecules.[38-39,42] This possible distortion in the 1*s*→3*d* pre-edge transitions during electron transfer (Fe(III) → Fe(II)) in the octahedral coordination environment, may explain the intensity gain observed for Fit_Fe(II&III) as a result of their quadrupolar character.[38,40-41] This finding corroborates the initial EPR observations. Furthermore, the Fe(III)CaM and Fit_Fe(II&III) spectra appear to align with the standard Fe(III) spectrum, both in the 1*s*→4*s* (main-edge) and in the 1*s*→3*d* (pre-edge) transition regions, demonstrating a 100% Fe(III) composition in the pre-phenol-dosed sample (Fe(III)CaM) with no distortion in the coordination environment. In summary, the XANES data support the proposal that phenol is chemisorbed to the Fe redox centre and, via electron donation, reduces Fe(III) to Fe(II),and reinforce the EPFR formation mechanism presented in Scheme 1.

Radical Density: The combination of ICP-OES and XANES results allows for an estimation of the Fe(II) concentration (in atoms per gram), while EPR analysis allows for the determination of spins (EPFRs) per gram. Thus, by linking the data from these three techniques, one can obtain an estimate of EPFR density per Fe(II) atom (in spins /atom). Remarkably, it was found that there were 1.5×10^{-2} spins/Fe(II) atom. Stated differently, only 3 EPFRs are produced per 200 Fe(III) atoms reduced (or 200 electrons transferred). While steric effects between metal atoms have been reported to be the biggest factor affecting the accessibility of phenol to the transition metal surface,[11] steric effects due to phenol orientation on the metal surface are bound to affect the lifetime of the radical as well, increasing the chances of radical recombination and decay. Thus, the low ratio of EPFRs to Fe(II) redox centres reported here can be explained by a large number of the initially formed radicals combining with other radicals in the areas of high radical density—in short, phenoxyl radical polymerization— leading to the relatively rare event of long-lived EPFR formation in the areas of low radical density.

3.5 Influence of Fe(III) Loading in Fe(III)CaM on EPFR Concentration

To further investigate the relationship between Fe concentration and EPFR formation, Fe(III)CaM samples with different Fe loadings were prepared from Fe solutions of varying concentrations, ranging from 0.0021 *M* to 0.025 *M*, following previously stated procedures.[19] Upon exposure to phenol, an increase in the Fe(III) loading concentration from ~8×10^3 mg/kg to ~2.4×10^4 mg/kg caused a non-linear increase in the EPFR concentration (*cf.* Fig. 6A). EPFR concentrations obtained when the Fe loading concentrations were between ~ 1.8×10^4 and 2.4×10^4 mg/kg were found to be statistically within the same range. This observation can be explained as follows: at low Fe loadings (8×10^3 mg/kg – 1.0×10^4 mg/kg) only a few Fe(III) centres are available for EPFR formation. Due to steric effects, the adsorbed phenoxyl radicals prevent additional phenol molecules from accessing Fe(III) centres.[11] However, at higher Fe loading concentrations (> 1.0×10^4 mg/kg), more and more Fe(III) centres become available for reaction with phenol. The data also show that, at 1.8×10^4 mg/kg, an optimum number of the appropriate Fe(III) centres are available, beyond which no further EPFR formation occurs. This EPFR saturation can be explained by the fact that, at higher (1.8×10^4 mg/kg) Fe(III) concentrations, there are either no additional isolated Fe(III) centres, causing any radicals formed to react with each other instead of facilitating EPFR formation or additional Fe(III) are not accessible to sorbed phenol molecules due to steric reasons.

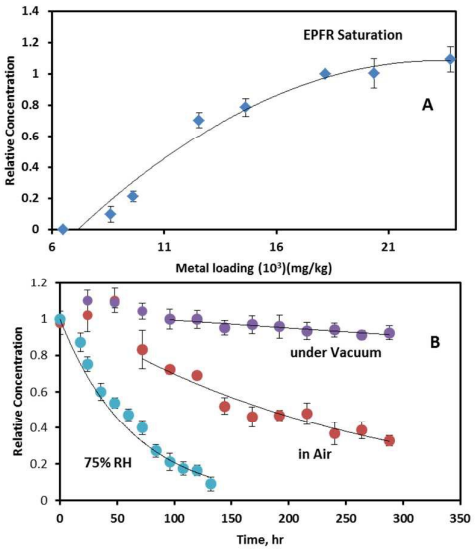

Fig. 6 A) Relationship between EPFR concentration and Fe(III) loading concentration B) EPFR lifetimes for DosedFe(III)CaM in vacuum (purple), after exposure to ambient air (red) and at 75% relative humidity (RH; blue).

This journal is © The Royal Society of Chemistry 20xx

Please do not adjust margins

Environmental Science: Processes & Impacts Accepted Manuscript

3.6 EFPR Lifetime Analysis

The stability of EPFRs in the atmosphere contributes to their environmental impact. We have investigated this by exposing the Fe(III)CaM-associated EFPRs to air.

Effect of Air on EPFR Persistence: EPFR lifetimes have been widely studied as a way to express their persistency and stability after exposure to molecular oxygen in the environment.[11,16,43] The EPFR concentrations in DosedFe(III)CaM samples (at an approximate $1.8x10^4$ mg/kg Fe(III) loading concentration) were monitored immediately upon exposure to air and under relative humidity (RH) range of 22%–38%, both in the dark (to minimize the chance of a photoreaction). The same procedures were carried out with EPFRs under vacuum to serve as a control experiment for an oxygen-free atmosphere. The results for these experiments are shown in Fig. 6B with two time periods being apparent: the growth period, during which EPFRs were formed, and the subsequent decay period. The growth period is attributed to the migration of phenol to more active Fe(III) sites in the clay.

The growth period also resulted in the g-factor and Δ*Hp-p* of the EPFRs increasing from 2.0034 to 2.0036 and from 6.1 to ~6.6–6.9 G, respectively. The increase in Δ*Hp-p* is a consequence of concentration broadening.[37] The EPFR decay rates and lifetimes were determined employing the pseudo-first-order integrated rate law expression ($ln\,(R/R_0) = -kt$, where $t_\tau = 1/k$, τ =1/e, e is the base of the natural logarithm, and R/R_0 is the ratio of the final to initial radical concentrations).[11,16,43] When suspended in vacuum, EPFRs showed significant stability, with decay occurring at a very slow rate of 0.00028 h^{-1}, yielding a 1/e lifetime of τ = 148.8 days . During this decay period, the g-factor and Δ*Hp-p* remained unchanged. For EPFR decay monitored in air, a 1/e lifetime of 10.4 days was observed with a decay rate of 0.0040 h^{-1}. During the in-air decay period, the g-factor and Δ*Hp-p* decreased to 2.0032 and 5.2 G, respectively. The total EPFR lifetimes for the systems under study here are 151.8 days (with 72 h of radical growth) under vacuum compared to 12.4 days (with 48 h of radical growth) in air.

The above lifetimes are longer than the 3.8 days previously reported for EPFRs generated (in air) on a $Fe(III)_2O_3$/silica system, a model surrogate of the $PM_{2.5}$ system,[16] dosed with phenol at 230 °C, but shorter than those reported for EPFRs in pentachlorophenol-contaminated soils and real $PM_{2.5}$ systems. Conversely, multiple decays with longer combined EPFR lifetimes of 39 and 21− 5028 days were reported for PCP-contaminated soil and real $PM_{2.5}$ systems, respectively.[37,43] The complex nature of the soil matrix, which can consist of polymeric aromatic components of soil organic matter (SOM) and assorted transition metals (Fe(III), Cu(II), Mn(III)),[13-14,36,43] may account for the longer lifetimes encountered in the contaminated soil system due to local effects, such as hydrophobic associations and π-stacking, which are common with the SOM systems.[13-14,43] Additionally, the long EPFR lifetimes for real $PM_{2.5}$ samples have been previously explained by the presence of trapped EPFRs, also known as 'internal radicals'. This trapping, or internalization, protects radicals from molecular oxygen in the environment, hindering the oxidation, and hence, slowing decay processes of these 'internal' EPFRs.[37] It has also been reported that phenol intercalation can occur in a montmorillonite clay containing organic cations, constricting phenol molecules to their interlayer domain.[44] The same intercalation can be assumed for the system under study here, as evidenced by the increase of the basal spacing from 1.31 nm to 1.45 nm for Fe(III)CaM and DosedFe(III)CaM (*cf.* Fig. 1), causing similar internalization and hindrance to oxidation, resulting in longer EPFR lifetimes for the DosedFe(III)CaM than for the $Fe(III)_2O_3$/silica system. Radical dimerization provides another plausible explanation of the prolonged EPFR lifetimes, especially during the radical growth period after air exposure.[43] For example, a cyclopentadienyl radical formed from a phenoxyl radical via chlorophenoxyl radical intermediates, was previously implicated in the formation of different types of dioxins.[16] Such an occurrence may can also contribute to the slight change in the g-factor and Δ*Hp-p* observed during the radical growth period in this work.

Effect of Humidity on EPFRs Persistence: The observed EPFR decay after exposure to air may also be due to the adsorption of water molecules to, and desorption of the organic precursor from active metal sites. To verify this assertion, DosedFe(III)CaM EPFRs were exposed for 4 h to 75% RH air at 25 °C and their decay was monitored. As shown in Fig. 6B, a much faster decay rate of 0.02 h^{-1} was found under these conditions, amounting to a 1/e lifetime of 2.1 days and no initial growth period. During the EPFR decay period, the g-factor decreased from the 2.0033 – 2.0035 range to 2.0030, while the Δ*Hp-p* showed a swift decrease from 6.2 to 4.7 G, suggesting a more homogenous radical system.[20] The increase in the RH of air to 75% resulted in EPFRs decaying 5 times faster than in air with RH ranging from 22% to 38%, and 71 times faster than under vacuum. This observation suggests that humidity is a more important factor than the presence of oxygen in the EPFR decay processes taking place in the environment. Additionally, at 75% RH conditions, no prolonged growth period was observed, presumably due to the water molecules blocking all available active Fe(III) sites, inhibiting further reaction.

4. Conclusions

It has previously been found that soils with iron concentrations between 14 and 23 × 10^3 mg/kg, contaminated with phenols and, to a lesser extent, other organic pollutants, have EFPR concentrations ranging from 5.83 × 10^{17} to 20.2 × 10^{17} spins/g.[13] The complex tri-component biological/mineral/SOM soil system is an analytical challenge, especially for mechanistic studies. This study is an initial step in gaining a mechanistic understanding of how EPFR form in contaminated soils by simplifying the soil system to its mineral components. The mineral component, represented here by montmorillonite clay, was chosen as it has been shown that the vast majority of EPFRs in contaminated soils are associated with this fraction, and that clay systems act as a major metal repository and a sorbent of organic pollutants.[13-14,43] This model system yielded EPFR concentrations and lifetimes close to, but lower than those reported for real world soil samples, with no biological component present. The differences in concentration can be explained by other processes, such as enzyme-enhanced EPFR formation.[13,14] The longer EPFR lifetimes for real world soil samples can be explained by SOM stabilization, as we have previously suggested.[14]

Environmental Science: Processes & Impacts Accepted Manuscript

Please do not adjust margins

Mechanistically, the Fe-loaded montmorillonite system revealed that, under environmentally relevant conditions, an EPFR can be formed by the intercalation sorption of phenol, followed by a transfer of an electron from the phenol to an Fe(III) centre, which results in the reduction of iron to Fe(II). The intercalation of phenol results in the intercalated EPFR, which reduces the ability of oxygen to oxidize this radical, and hence, allows for a long-lived radical. This mechanism can be further extended by the fact that the concentration of EPFRs (spins) are much lower than that of the Fe(II) centres per gram of clay, which leads to the conclusion that a large number of the formed radicals dimerize and form non-radical final products, such as dioxins, and only the isolated radicals become EPFRs. Finally, it was found that high humidity resulted in faster EPFR decay, hence EPFR toxicity may be lower in humid climates.

The strong resistance to oxidation and the stability of these radicals after exposure to air imply that, even without the stabilizing effect of SOM, the formed EPFRs can persist long enough in the soil to increase the chance of the EPFR-containing clay particles being suspended in air by wind and, in turn, inhaled, ultimately causing oxidative stress.[7] The critical environmental implication of this work lies in the observation that the clay system, when contaminated, in the absence of any biological components, can form EPFRs at concentrations close to those found in real contaminated soils at ambient temperature, which has wide ranging environmental and human health implications, especially when humidity is relatively low.

Acknowledgements

Support for this research was provided by a grant from the NIEHS Superfund Research Program through grant, 2P42ES013648-03

Notes and references

1 H. Holmstrand, D. Gadomski, M. Mandalakis, M. Tysklind, R. Irvine, P. Andersson and Ö. Gustafsson, *Environmental Science & Technology*, 2006, **40**, 3730-3735.
2 C. Gu, C. Liu, C. T. Johnston, B. J. Teppen, H. Li and S. A. Boyd, Environmental Science & Technology, 2011, **45**, 1399-1406.
3 Y. Soma and M. Soma, *Environmental Health Perspectives*, 1989, **83**, 205-214.
4 T. Kunisue, S. Nakanishi, N. Oka, F. Sato, M. Tsurumi and S. Tanabe, *Environmental Science & Technology*, 2006, **40**, 6919-6927.
5 N. Ferré-Huguet, M. Nadal, M. Schuhmacher and J. L. Domingo, *Environmental Science & Technology*, 2005, **40**, 61-66.
6 B. Dellinger, W. A. Pryor, R. Cueto, G. L. Squadrito, V. Hegde and W. A. Deutsch, *Chemical Research in Toxicology*, 2001, **14**, 1371-1377.
7 M. A. Kelley, V. Y. Hebert, T. M. Thibeaux, M. A. Orchard, F. Hasan, S. A. Cormier, P. T. Thevenot, S. M. Lomnicki, K. J. Varner, B. Dellinger, B. M. Latimer and T. R. Dugas, *Chemical Research in Toxicology*, 2013, **26**, 1862-1871.
8 H. Truong, S. Lomnicki and B. Dellinger, *Chemosphere*, 2008, **71**, 107-113.
9 S. Lomnicki, H. Truong, E. Vejerano and B. Dellinger, *Environmental Science & Technology*, 2008, **42**, 4982-4988.
10 H. Truong, S. Lomnicki and B. Dellinger, *Environmental Science & Technology*, 2010, **44**, 1933-1939.
11 L. W. Kiruri, L. Khachatryan, B. Dellinger and S. Lomnicki, *Environmental Science & Technology*, 2014, **48**, 2212-2217.
12 Z. Sun, B. Tang and H. Xie, *Energy & Fuels*, 2015, **29**, 1269-1278.
13 A. L. N. dela Cruz, R. L. Cook, B. Dellinger, S. M. Lomnicki, K. C. Donnelly, M. A. Kelley and D. Cosgriff, *Environmental Science: Processes & Impacts*, 2014, **16**, 44-52.
14 A. L. N. dela Cruz, W. Gehling, S. Lomnicki, R. Cook and B. Dellinger, *Environmental Science & Technology*, 2011, **45**, 6356-6365.
15 S. A. Boyd and M. M. Mortland, *Environmental Science & Technology*, 1986, **20**, 1056-1058.
16 E. Vejerano, S. Lomnicki and B. Dellinger, *Environmental Science & Technology*, 2010, **45**, 589-594.
17 J. M. Tront, B. K. Amos, F. E. Löffler and F. M. Saunders, *Environmental Science & Technology*, 2006, **40**, 529-535.
18 F. Fu, D. D. Dionysiou and H. Liu, Journal of Hazardous Materials, 2014, **267**, 194-205.
19 Y.-L. Ma, Z.-R. Xu, T. Guo and P. You, *Journal of Colloid and Interface Science*, 2004, **280**, 283-288.
20 U. G. Nwosu and R. L. Cook, *Environ Eng Sci*, 2015, **32**, 14-22.
21 P. J. Wallis, A. L. Chaffee, W. P. Gates, A. F. Patti and J. L. Scott, *Langmuir*, 2010, **26**, 4258-4265.
22 N. H. Tran, M. A. Wilson, A. S. Milev, G. R. Dennis, G. S. K. Kannangara and R. N. Lamb, *Science and Technology of Advanced Materials*, 2006, **7**, 786-791.
23 M. A. Martinluengo, H. Martinscarvalho, J. Ladriere and P. Grange, *Clay Minerals*, 1989, 24, 495-504.
24 Z. Huang, P. Wu, H. Li, W. Li, Y. Zhu and N. Zhu, RSC Advances, 2014, **4**, 6500-6507.
25 A. Popov, E. Kondratieva, J.-P. Gilson, L. Mariey, A. Travert and F. Maugé, Catalysis Today, 2011, 172, 132-135.
26 D. R. Katti, K. S. Katti, M. Raviprasad and C. Gu, Journal of Nanomaterials, 2012, 2012, 15.
27 H. Qing-Qing, W. Guang-Wei, L. Zhao-Tie and L. Zhong-Wen, in Nanocatalysis for Fuels and Chemicals, American Chemical Society, 2012, vol. 1092, ch. 11, pp. 167-193.
28 L. V. Amorim, C. M. Gomes, H. d. L. Lira, K. B. França and H. C. Ferreira, Materials Research, 2004, 7, 583-593.
29 Y.-Q. Ji, L. Black, P. G. Weidler and M. Janek, Langmuir, 2004, 20, 9796-9806.
30 A. E. I. Elkhalifah, T. Murugesan and M. A. Bustam, 2011.
31 J. Madejová, Vibrational Spectroscopy, 2003, 31, 1-10.
32 K. Flogeac, E. Guillon and M. Aplincourt, *Journal of Colloid and Interface Science*, 2005, **286**, 596-601.
33 R. S. Muralidhara, C. R. Kesavulu, J. L. Rao, R. V. Anavekar and R. P. S. Chakradhar, *Journal of Physics and Chemistry of Solids*, 2010, **71**, 1651-1655.
34 J. Manjanna, T. Kozaki, N. Kozai and S. Sato, *Journal of Nuclear Science and Technology*, 2007, **44**, 929-932.
35 Z. Huang, P. Wu, H. Li, W. Li, Y. Zhu and N. Zhu, RSC Advances, 2014, 4, 6500-6507.
36 B. Dellinger, S. Lomnicki, L. Khachatryan, Z. Maskos, R. W. Hall, J. Adounkpe, C. McFerrin and H. Truong, Proceedings of the Combustion Institute, 2007, 31, 521-528.
37 W. Gehling and B. Dellinger, Environmental Science & Technology, 2013, 47, 8172-8178.
38 T. E. Westre, P. Kennepohl, J. G. DeWitt, B. Hedman, K. O. Hodgson and E. I. Solomon, Journal of the American Chemical Society, 1997, 119, 6297-6314.
39 P.-E. Petit, F. Farges, M. Wilke and V. A. Sole, *Journal of Synchrotron Radiation*, 2001, **8**, 952-954.
40 L. Galoisy, G. Calas and M. A. Arrio, *Chemical Geology*, 2001, **174**, 307-319.

Environmental Science: Processes & Impacts Accepted Manuscript

This journal is © The Royal Society of Chemistry 20xx

41 D. I. Ellery, M. D. Julia, F. L. Amelia, O. Michelle, F. Lydia, V. Stefan, L. Barry, L. Y. Patricia, S. T. Benjamin and A. B. Jay, *Nature Communications*, 2013, **4**.
42 G. S. Pokrovski, J. Schott, F. Farges and J.-L. Hazemann, *Geochimica et Cosmochimica Acta*, 2003, **67**, 3559-3573.
43 A. L. N. d. Cruz, R. L. Cook, S. M. Lomnicki and B. Dellinger, Environmental Science & Technology, 2012, 46, 5971-5978.
44 T. Okada, Y. Watanabea and M. Ogawa, Chemical Communications, 2004, DOI: 10.1039/b312962d, 320-321.

Environmental Science: Processes & Impacts Accepted Manuscript

Please do not adjust margins